Genetic Nicotinamide *N*-Methyltransferase (*Nnmt*) Deficiency in Male Mice Improves Insulin Sensitivity in Diet-Induced Obesity but Does Not Affect Glucose Tolerance

Sebastian Brachs,[1,2,3] James Polack,[1,2,3] Maria Brachs,[1,3] Kerstin Jahn-Hofmann,[4] Ralf Elvert,[4] Anja Pfenninger,[4] Felix Bärenz,[4] Daniel Margerie,[4] Knut Mai,[1,2,3,5] Joachim Spranger,[1,2,3,5] and Aimo Kannt[4,6]

Diabetes 2019;68:527–542 | https://doi.org/10.2337/db18-0780

Antisense oligonucleotide knockdown (ASO-KD) of nicotinamide *N*-methyltransferase (NNMT) in high-fat diet (HFD)–fed mice has been reported to reduce weight gain and plasma insulin levels and to improve glucose tolerance. Using NNMT-ASO-KD or NNMT knockout mice ($NNMT^{-/-}$), we tested the hypothesis that *Nnmt* deletion protects against diet-induced obesity and its metabolic consequences in males and females on obesity-inducing diets. We also examined samples from a human weight reduction (WR) study for adipose *NNMT* (a*NNMT*) expression and plasma 1-methylnicotinamide (MNAM) levels. In Western diet (WD)–fed female mice, NNMT-ASO-KD reduced body weight, fat mass, and insulin level and improved glucose tolerance. Although $NNMT^{-/-}$ mice fed a standard diet had no obvious phenotype, $NNMT^{-/-}$ males fed an HFD showed strongly improved insulin sensitivity (IS). Furthermore, $NNMT^{-/-}$ females fed a WD showed reduced weight gain, less fat, and lower insulin levels. However, no improved glucose tolerance was observed in $NNMT^{-/-}$ mice. Although *NNMT* expression in human fat biopsy samples increased during WR, corresponding plasma MNAM levels significantly declined, suggesting that other mechanisms besides a*NNMT* expression modulate circulating MNAM levels during WR. In summary, upon NNMT deletion or knockdown in males and females fed different obesity-inducing diets, we observed sex- and diet-specific differences in body composition, weight, and glucose tolerance and estimates of IS.

Nicotinamide *N*-methyltransferase (NNMT) is expressed in most tissues including skeletal muscle (SKM), fat, and liver (1–3). In humans, *NNMT* expression is highest in the liver, followed by fat, whereas in mice, adipose expression appears to exceed that of the liver by at least 10-fold (3,4). NNMT is highly expressed in several human cancers (5). It catalyzes methylation of nicotinamide (NAM) and other pyridine derivatives using *S*-adenosylmethionine (SAM) to yield the products 1-methylnicotinamide (MNAM) and *S*-adenosylhomocysteine (SAH). NNMT may play a role in the biotransformation of xenobiotics (6,7). NAM is the amide of nicotinic acid, and together these are known as niacin/vitamin B3. After the methylation of NAM to MNAM, it no longer functions as an NAD^+ precursor and can be excreted via urine (8,9). Increased urinary concentration of MNAM has been shown in humans with type 2 diabetes (T2D) and obesity-prone mouse strains (10). SAM is a methyl donor in numerous reactions catalyzed by methyltransferases including histone methylation, which can affect gene regulation and metabolism (11).

In high-fat diet (HFD)–fed mice, adipose NNMT protein (12), mRNA (13), and enzyme activity (4) were increased.

[1]Department of Endocrinology and Metabolism, Charité–Universitätsmedizin Berlin, Berlin, Germany
[2]DZHK (German Centre for Cardiovascular Research), partner site Berlin, Germany
[3]Center for Cardiovascular Research (CCR), Charité–Universitätsmedizin Berlin, Berlin, Germany
[4]Sanofi Research and Development, Frankfurt am Main, Germany
[5]Clinical Research Unit, Berlin Institute of Health (BIH), Berlin, Germany
[6]Institute of Experimental and Clinical Pharmacology and Toxicology, Medical Faculty Mannheim, Heidelberg University, Mannheim, Germany

Corresponding author: Joachim Spranger, joachim.spranger@charite.de, or Aimo Kannt, aimo.kannt@sanofi.com

Received 29 July 2018 and accepted 3 December 2018

Clinical trial reg. no. NCT00850629, clinicaltrials.gov

This article contains Supplementary Data online at http://diabetes.diabetesjournals.org/lookup/suppl/doi:10.2337/db18-0780/-/DC1.

S.B., J.P., J.S., and A.K. contributed equally to this work.

Human adipose *NNMT* (a*NNMT*) expression appears to be increased in T2D and to correlate negatively with insulin sensitivity (IS) among individuals with diabetes (2); however, an association with obesity remains unclear (2,14). Investigations of a*Nnmt* and liver (l)*Nnmt* expression reveal a high interstrain variability in mice (~20-fold in white adipose tissue [WAT], ~150-fold in liver) and a similar intersubject variability in humans (2). Suggestive of a causative role of NNMT in the development of obesity and associated metabolic dysregulation, antisense oligonucleotide knockdown (ASO-KD) protected against these phenotypes by increasing cellular energy expenditure (EE) in HFD-fed mice (12). ASO-KD reduced *Nnmt* in liver and WAT and led to reduced weight gain, relative fat mass, plasma insulin levels, and plasma triglyceride levels and improved glucose tolerance (12).

Here, we aimed to broaden the body of knowledge regarding the role of NNMT in metabolic disease. With a constitutive knockout, we investigate the effects of *Nnmt* deletion on energy metabolism, glucose homeostasis, and the development of obesity. Furthermore, we examine a human weight reduction (WR) study for *NNMT* expression, MNAM levels, and changes of metabolic parameters.

RESEARCH DESIGN AND METHODS

Animal Experiments

NNMT knockout ($NNMT^{-/-}$) experiments were conducted according to institutional ethical guidelines and approved by LAGeSo (Landesamt für Gesundheit und Soziales) Berlin (G0276/15) and by personal licenses for Jacob Jelsing (2013-15-2934-00784) issued by the Danish Committee for Animal Research.

VelociGene (Regeneron Pharmaceuticals, Inc.) technology (15) was used to generate conditional $NNMT^{fl/fl}$ mice on a C57BL/6 background at Regeneron Pharmaceuticals Inc. Details of the targeting strategy are depicted in Fig. 3*A*. For whole-body *Nnmt* deletion, mice were crossbred with a ZP3-Cre deleter (C57BL/6-Tg(Zp3-cre)93Knw/J; The Jackson Laboratory).

$NNMT^{-/-}$ and wild-type littermate controls (WT) were shipped to Sanofi (Frankfurt am Main, Germany) or Charité–Universitätsmedizin Berlin (Berlin, Germany) for experiments.

The 6- to 10-week-old males or females were fed an HFD (fat 60% kcal; carbohydrate 20% kcal) (D12492; Research Diets, Inc.), a Western diet (WD) (fat 47% kcal; carbohydrate 34% kcal) (TD.97366; ssniff special diets GmbH), or a standard diet (STD) (Rat/Mouse-Maintenance; ssniff special diets GmbH) ad libitum (Supplementary Tables 5–7) with free access to water. Mice were maintained in individually ventilated cages (2–4/cage) environmentally controlled with a 12-h light/dark cycle and monitored weekly. Body composition was assessed by ^{1}H-MRS using a Minispec LF50 Body Composition Analyzer (Bruker BioSpin).

$NNMT^{-/-}$ and WT females were fed a WD for 18 weeks. From week 13 to 18, animals were treated daily with a vehicle (30% PEG200) by oral gavage to simulate pharmacological intervention with a test compound, analogous to another set of experiments (16), but not in weeks 1–12 of the WD, in which we assessed body composition, body weight (BW) gain, and food intake. In week 18, an oral glucose tolerance test (oGTT) was performed in PEG200-treated mice. In our article, we mainly used data from weeks 1–12 before PEG200 treatment.

C57BL/6N females (Taconic) were randomized into three groups receiving PBS (vehicle), control-ASO, or NNMT-ASO (37.5 mg/kg) (Supplementary Table 1) (taken from Kraus et al. [12]) subcutaneously every other day for 10 weeks on a WD. ASOs were partly 2′-*O*-(methoxy)-ethyl modified to improve resistance against nucleases, synthetized on a 250-μmol scale by phosphoramidite chemistry, purified using ion-exchange chromatography (Q Sepharose FF), desalted by ultrafiltration, and freeze dried, and purity was determined by reverse-phase high-performance liquid chromatography (>90%). Control- and NNMT-ASO were detected as free acids by their masses of 7215.6 and 7251.9 Da.

GTTs were performed in overnight-fasted (16 h) mice orally applying 2 g (WD) or intraperitoneally applying 1 g/2 g (HFD/SD) glucose/kg BW. Glucose and insulin (oGTT only 15 min value) were measured at 0, 15, 30, 60, and 120 min via the tail.

Hyperinsulinemic-euglycemic (HE) clamps in conscious, restrained mice and activity and indirect calorimetry (TSE LabMaster System) were performed as described previously (17).

Terminally, mice were sacrificed, and samples were analyzed, collected, immediately processed, and/or appropriately stored. Detailed information for mouse phenotyping is summarized in Table 1.

Biochemical Analysis

Western blot of epididymal WAT (eWAT) using Total OXPHOS WB-Antibody-Cocktail (ab110413; Abcam), rabbit-anti-mouse NNMT (ARP42281_T100; Aviva Systems Biology), rabbit-anti-mouse α-tubulin (2144; NEB), and horseradish peroxidase–anti-rabbit IgG (7074; Cell Signaling Technology) for detection was conducted as described previously (18,19). Optical density (OD) was quantified by ImageJ (20).

Plasma glucose was measured in duplicate (≤10%) with Contour XT glucometer (Ascensia), nonesterified fatty acids (NEFAs) by NEFA HR (2) kit (FUJIFILM Wako Diagnostics U.S.A.), insulin via Mouse Insulin ELISA Kit (Mercodia), and other metabolic parameters on a Cobas 6000c (501-module; Roche Diagnostics) according to manufacturer instructions using the following: Autokit Total Ketone Bodies (FUJIFILM Wako Diagnostics U.S.A.), Glucoquant Glucose/HK Kit, cholesterol with CHOD-PAP kit, and Crep2 Creatinine plus V2 (all Roche Diagnostics).

Plasma/tissue MNAM levels were measured by a liquid chromatography-tandem mass spectroscopy method with chromatographic separation and quantification as described previously (2).

Mouse/human RNA was extracted using TRIzol, DNase digested, and transcribed into cDNA via RevertAid Reverse

Table 1—Detailed information for metabolic phenotyping

Experiments	Sex	Diet	Diet length (weeks)	Age (weeks)	Fasting (h)	Specifications
NNMT-ASO						
BW	F	WD	10	6–8	No	Food and water access ad libitum, scoring weekly
GTT	F	WD	10	16–18	16	2 mg glucose/g BW, oral
Sacrifice	F	WD	11	16–18	None	Cervical dislocation; collection of liver, scWAT, vWAT, and plasma; immediate storage in nitrogen and −80°C
$NNMT^{-/-}$						
BW	M	STD	15	6–8	No	Food and water access ad libitum, scoring weekly
GTT	M	STD	18	26–28	16	2 mg glucose/g BW, i.p.
Metabolic cage	M	STD	17	25–27	None	Adaption period: 24 h, measurements: 48 h (as mean for 24 h)
Catheterization	M	STD	15	23–25	None	Vena jugularis, 7 days recovery
HE clamp	M	STD	16	24–26	16+	Conscious, restrained, sampling from tail; insulin priming 21.4 mU/kg and constant infusion rate 3 mU/kg/min insulin; [3-^{3}H]-D-glucose (infusion rates: basal 0.05 μCi/min and clamp 0.1 μCi/min) and 2-deoxy-[^{14}C]-D-glucose (bolus: 10 μCi)
Sacrifice	M	STD	22	30–32	None	Clamped mice: in anesthesia with ketamine/xylazine mix i.v.; collection of GAS, EDL, QD, eWAT, liver, heart, BAT, plasma; immediate storage in nitrogen and −80°C Nonclamped mice: cervical dislocation; collection of GAS, QD, pancreas, spleen, kidney, eWAT, scWAT, liver, heart, BAT, plasma; immediate storage in nitrogen and −80°C
BW	M	HFD	10	6	No	Food and water access ad libitum, scoring weekly
GTT	M	HFD	10	16	16	1 mg glucose/g BW, i.p.
Metabolic cage	M	HFD	10	16	None	Adaption period: 24 h, measurements: 48 h (as mean for 24 h)
Catheterization	M	HFD	11	17	None	Vena jugularis, 7 days recovery
HE clamp	M	HFD	12	18	16	Conscious, restrained, sampling from tail; insulin priming 21.4 mU/kg and constant infusion rate 3 mU/kg/min insulin; [3-^{3}H]-D-glucose (infusion rates: basal 0.05 μCi/min and clamp 0.1 μCi/min) and 2-deoxy-[^{14}C]-D-glucose (bolus: 10 μCi)
Sacrifice	M	HFD	13	19	None	Clamped mice: in anesthesia with ketamine/xylazine mix i.v.; collection of GAS, EDL, QD, eWAT, liver, heart, BAT, plasma; immediate storage in nitrogen and −80°C Nonclamped mice: cervical dislocation; collection of GAS, QD, pancreas, spleen, kidney, eWAT, scWAT, liver, heart, BAT, plasma; immediate storage in nitrogen and −80°C
BW	F	WD	12	6–8	No	Food and water access ad libitum, scoring and food intake per cage weekly
GTT	F	WD	18	24–26	16	2 mg glucose/g BW, oral
Sacrifice	F	WD	19	25–27	None	Cervical dislocation; collection of liver, scWAT, vWAT, plasma; immediate storage in nitrogen and −80°C

BAT, brown adipose tissue; EDL, extensor digitorum longus; F, female; GAS, gastrocnemius; GTT, glucose tolerance test; i.v., intraveneous; M, male; QD, quadriceps vastus lateralis.

Transcriptase as described previously (17). Quantitative real-time PCR was performed on a Roche LightCycler 96 (Roche Diagnostics). Human/mouse *NNMT/Nnmt* expression was normalized to cyclophilin (*PPIA/Ppia*), *GAPDH/Gapdh*, and/or β-actin (*Actb*). For the primers used, see Supplementary Table 8.

RNA of five liver samples of $NNMT^{-/-}$ and WT mice (fed for 12 weeks with an HFD) was isolated using RNeasy Plus Universal kit (Qiagen) according to the manufacturer protocol. The 100 ng/μL RNA samples (RNA integrity number >7, $OD_{260/280}$ ≥2.0, $OD_{260/230}$ ≥1.6) were prepared for next-generation RNA sequencing. RNA library preparation using the Illumina TruSeq RNA Sample Prep Kit V2 including polyA selection and single-end sequencing (50 base pairs, adaptor trimming, demultiplexing) were performed on an Illumina HiSeq 2500 System on High Output Run Mode at ATLAS Biolabs. Summarized results are in Supplementary Table 9.

Clinical Study

Study protocols were approved by the Institutional Review Board of Charité–Universitätsmedizin Berlin. It is registered under NCT00850629 (clinicaltrials.gov). All subjects gave written informed consent (21,22). Briefly, obese subjects were anthropometrically and metabolically phenotyped (oGTT, calorimetry, bioimpedance, HE clamps) and subcutaneous WAT (scWAT)/SKM biopsy samples were taken before (T-3) and after (T0) 3 months of WR through lifestyle intervention and analyzed by RNA sequencing to discover differentially expressed genes (23).

Data and Statistical Analyses

All data are presented as the mean ± SD or Tukey box-and-whisker plots. Whiskers represent the range except where data lie >1.5 interquartile ranges above/below the

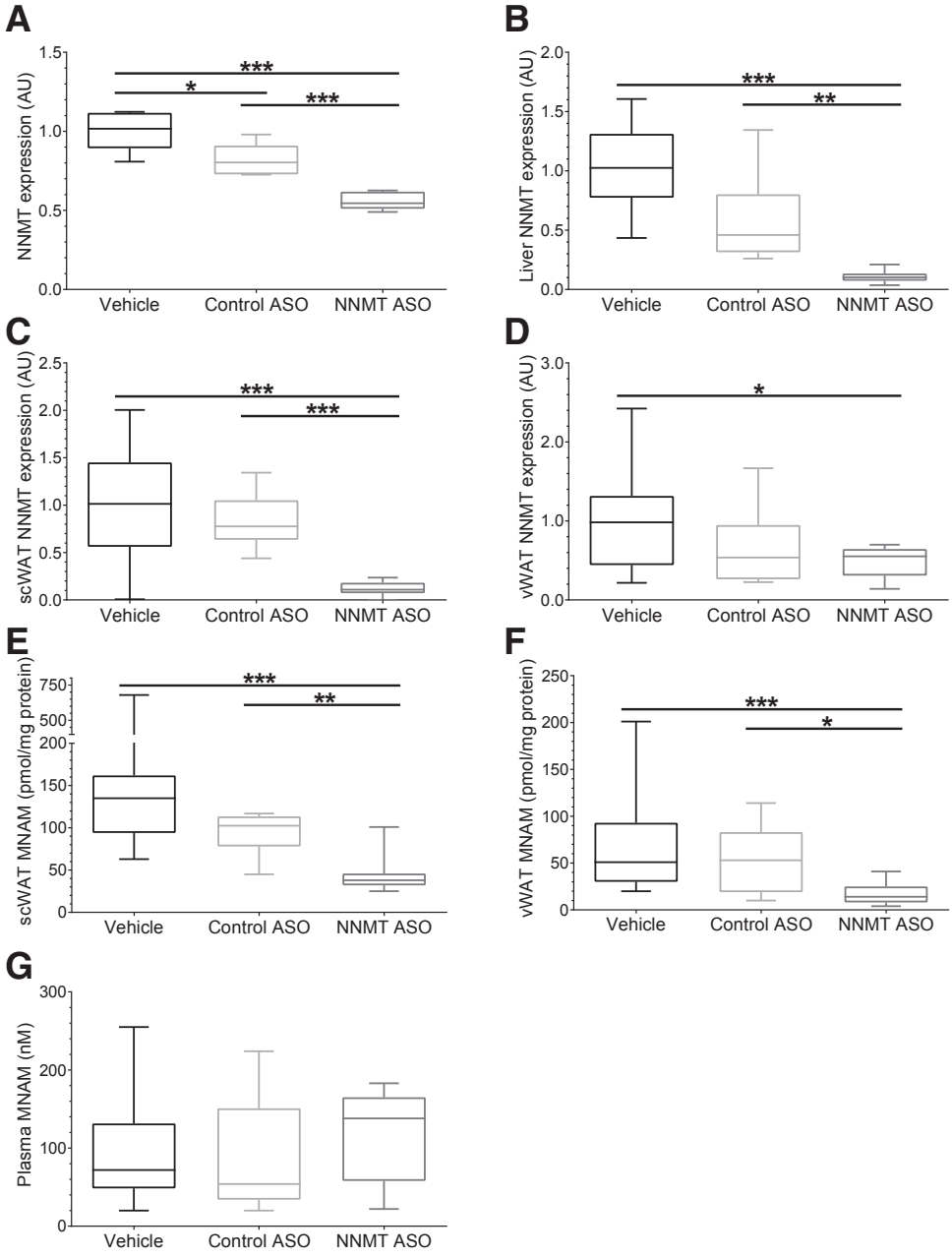

Figure 1—*Nnmt* knockdown with ASO treatment. *A*: *Nnmt* expression in *3T3-L1* adipocytes normalized to *β-actin* after 48 h of treatment with vehicle, control-ASO, or NNMT-ASO. *B–G*: *Nnmt* expression and MNAM in tissue and plasma were determined after 10 weeks of treatment with vehicle, control-ASO, or NNMT-ASO in mice fed a WD. *B*: *Nnmt* expression in liver tissue normalized to *β-actin*. *Nnmt* expression in scWAT (*C*) and in vWAT (*D*) normalized to *Gapdh*. MNAM concentration per milligram of protein in scWAT (*E*) and in vWAT (*F*). *G*: MNAM concentration (nM) in plasma. $^{*}P \leq 0.05$, $^{**}P \leq 0.01$, $^{***}P \leq 0.001$. Statistical significance was calculated using one-way ANOVA with Tukey mct (*A*, *C*, and *D*) or Kruskal-Wallis test by ranks with Dunn mct (*B* and *E–G*). Data represent Tukey boxplots. *N* = 6 (*A*); *N* = 9–12 (*B–G*). *N* values are stated per treatment group. AU, arbitrary units.

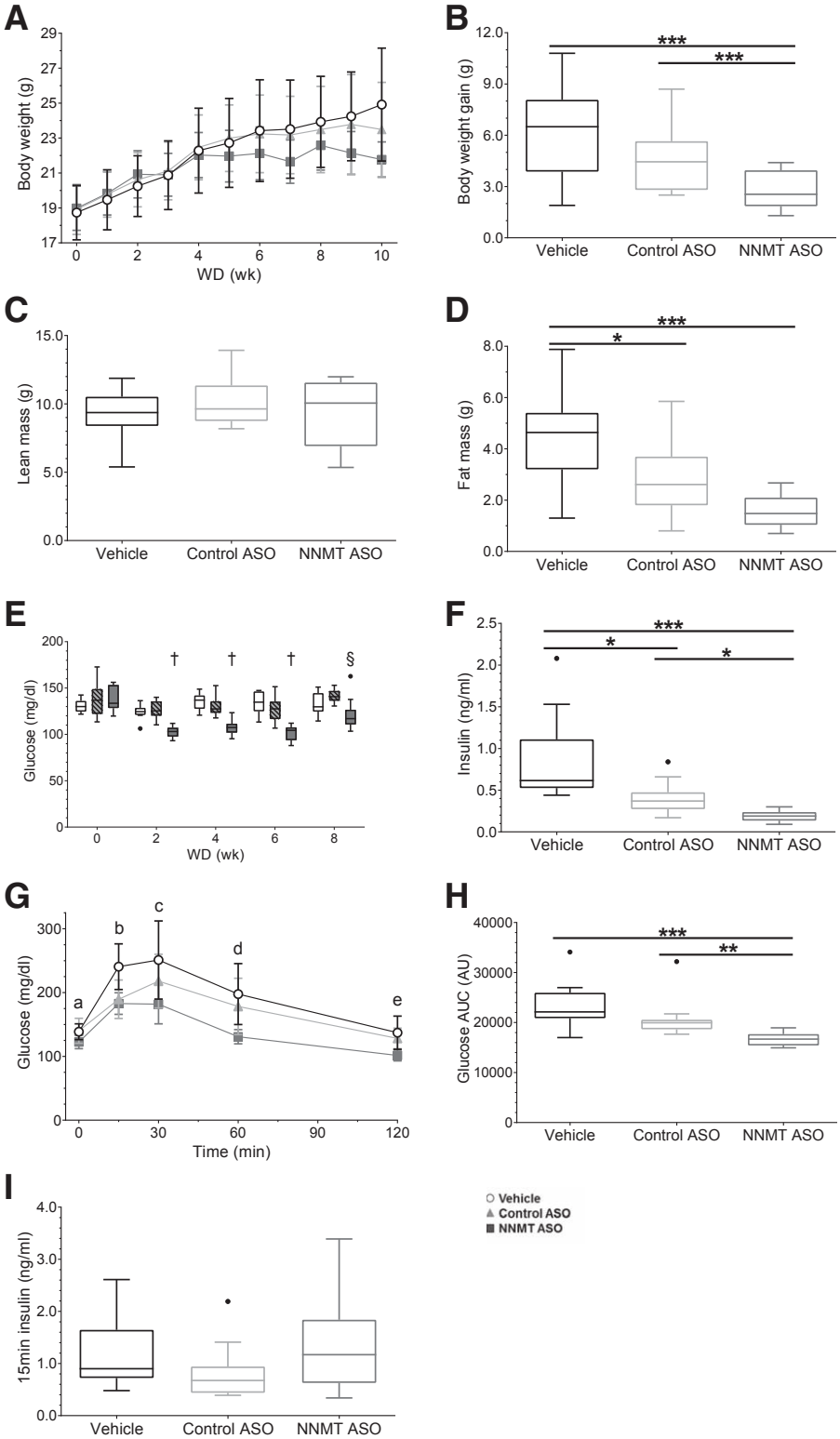

Figure 2— BW, body composition, and parameters of glycemic control during 10 weeks of NNMT-ASO treatment in female mice fed a WD. *A*: BW progression during 10 weeks of treatment, NNMT-ASO vs. vehicle or control-ASO. *B*: Total BW gain. *C*: Lean mass after 10 weeks. *D*: Fat mass after 10 weeks. *E*: Ad libitum–fed glucose concentration in plasma after 0, 2, 4, 6, and 8 weeks. †$P < 0.0001$ vs. vehicle and control-ASO; §$P < 0.0001$ vs. vehicle/$P = 0.02$ vs. control-ASO. *F*: Plasma insulin concentration in an ad libitum–fed state after 10 weeks. *G*: Plasma glucose concentration during an oGTT performed after 10 weeks; a, nonsignificant (ns); b, NNMT-ASO vs. vehicle $P < 0.0001$/NNMT-ASO vs. control-ASO ns/vehicle vs. control-ASO $P = 0.004$; c, NNMT-ASO vs. vehicle $P < 0.0001$/NNMT-ASO vs. control-ASO $P = 0.02$/vehicle vs. control $P = 0.004$; d, NNMT-ASO vs. vehicle $P < 0.0001$/NNMT-ASO vs. control-ASO $P = 0.001$/vehicle vs. control ns; e, NNMT ASO vs. vehicle $P = 0.03$/NNMT-ASO vs. control-ASO ns/vehicle vs. control-ASO ns. *H*: Area under the oGTT glucose-time curve (AUC). *I*: Measurement of plasma insulin at 15 min within the oGTT. White circles/white boxes depict treatment with vehicle; gray triangles/striped

75th/25th percentile; outliers are depicted as black dots and are included in each analysis.

GraphPad Prism 6 (GraphPad Software, La Jolla, CA) and R version 3.1.1 (24) were used for statistics and graphs.

Statistical significance was considered as $^{*}P \leq 0.05$, $^{**}P \leq 0.01$, and $^{***}P \leq 0.001$. Differences were calculated using a two-tailed unpaired Student *t* test with Welch correction or Mann-Whitney test, one-way or two-way (repeated-measures) ANOVA adjusted with a Tukey or Bonferroni multiple-comparisons test (mct) for post hoc analysis, or Kruskal-Wallis test by ranks with Dunn mct. Correlations were calculated using Pearson or Spearman correlation coefficient, all depending on whether data passed the normal distribution tests.

Mouse RNA sequencing raw data were analyzed using Array Studio Software (OmicSoft Corporation, Cary, NC). RNA-sequencing reads (fastq files) were mapped to the mouse genome with OmicSoft gene model B38 (20141031) and OSA4 as aligner. The number of fragments per kilobase of transcript per million mapped reads (FPKM) and counts were calculated. Genes with FPKM <1 were filtered out according to the 50% fraction rule to exclude minimally expressed genes. As quality control assessment, principal component analysis was applied. Between WT and $NNMT^{-/-}$ mice, differentially expressed genes were detected using the DESeq2 package in SPSS with a cutoff of a >1.5 fold change in expression and $P < 0.05$ adjusted with Benjamini-Hochberg procedure to control false discovery rates. All differentially expressed genes are listed in Supplementary Table 4.

Human data were analyzed using R by two-tailed Wilcoxon matched-pairs signed rank test, paired two-way ANOVA adjusted with Bonferroni mct. Correlations were calculated by Spearman correlation with Bonferroni mct. A linear regression model was used and adjusted for confounders (age, sex, and BMI at T-3). Statistical tests were used appropriately; details are in figure legends.

RESULTS

NNMT-ASO-KD Reduced BW and Fat in WD-Fed Mice

We investigated the effects of NNMT-ASO-KD (Supplementary Table 1) on BW, body composition, and metabolic parameters in female mice fed a WD for 12 weeks. NNMT-ASO-KD reduced *Nnmt* expression in 3T3-L1 adipocytes (Fig. 1*A*) and in vivo in liver (Fig. 1*B*) and scWAT (Fig. 1*C*) compared with vehicle and control-ASO and in visceral WAT (vWAT) (Fig. 1*D*) compared with vehicle. MNAM concentration was reduced in scWAT (Fig. 1*E*) and vWAT (Fig. 1*F*) but not in plasma (Fig. 1*G*). During 10 weeks of WD, NNMT-ASO-KD mice showed no significantly reduced BW at any time point compared with vehicle or control-ASO mice (Fig. 2*A*); however, their cumulative weight gain was decreased (Fig. 2*B*). Although lean mass remained similar (Fig. 2*C*), NNMT-ASO mice gained less fat than vehicle and by trend compared with control-ASO mice (Fig. 2*D*). In mice fed ad libitum, plasma glucose was decreased throughout (Fig. 2*E*) and insulin was decreased at the end of WD in NNMT-ASO-KD mice (Fig. 2*F*). After 10 weeks, the NNMT-ASO–treated mice showed diminished glucose excursions in an oGTT (Fig. 2*G*) with a significantly lower area under the curve for glucose (Fig. 2*H*), but no difference in plasma insulin levels at 15 min (Fig. 2*I*). Having observed the beneficial effects of NNMT-ASO-KD on BW, fat, and glucose tolerance also in WD-fed mice, we next generated an *Nnmt* knockout.

Generation of Whole-Body $NNMT^{-/-}$ Mice

After the generation of conditional $NNMT^{fl/fl}$ mice (Fig. 3*A*), we crossbred them with a global ZP3-Cre deleter to generate whole-body *Nnmt* knockout mice ($NNMT^{-/-}$) and compared them to $NNMT^{fl/fl}xCre^{-}$ control littermates (i.e., WT). We validated the *Nnmt* deletion on DNA, RNA, and protein level (Fig. 3*B–D* and Supplementary Fig. 1*A* and *B*). Consistent with *Nnmt* deletion, MNAM concentration in $NNMT^{-/-}$ mice was reduced by >99% in plasma, liver, and vWAT (Fig. 3*E–H*), whereas the NAM concentration was increased in plasma but not in liver or vWAT (Fig. 3*I–K*), and plasma SAM and SAH remained unchanged (Fig. 3*L*).

Body Composition and Metabolic Parameters of Male $NNMT^{-/-}$ Mice on STD

Kraus et al. (12) aligned *Nnmt* expression data and mouse strains by their susceptibility for obesity and showed that increasing *Nnmt* in WAT but not in liver matched increasing susceptibility to develop obesity. Using a second data set from www.BioGPS.org containing additional strains and their a*Nnmt* expression, no such correlation (between expression and propensity for obesity) was observed (Supplementary Fig. 2). We first examined the potential effects of *Nnmt* deletion in the absence of any dietary challenge. We analyzed male $NNMT^{-/-}$ mice on STD for BW, body composition, and basal metabolic parameters including glucose and insulin. Furthermore, we investigated them by intraperitoneal glucose tolerance test (ipGTT); characterized their food and water intake, respiratory exchange ratio (RER), EE, locomotor activity, O_2 consumption, and CO_2 production in metabolic cages; and performed HE clamps to estimate IS by glucose infusion rate (GIR), endogenous glucose production (EGP), and rate of glucose disappearance (R_d). However, these investigations did not reveal differences between $NNMT^{-/-}$ and WT mice (Supplementary Table 2).

boxes treatment with control-ASO; gray squares/gray boxes treatment with NNMT-ASO. $^{*}P \leq 0.05$, $^{**}P \leq 0.01$, $^{***}P \leq 0.001$. Statistical significance was calculated using one-way ANOVA with Tukey mct (*C*, *D*, *H*, and *I*), Kruskal-Wallis test by ranks with Dunn mct (*B* and *F*), or two-way ANOVA with Bonferroni mct (*A*, *E*, and *G*). Data represent the mean ± SD (*A* and *G*) or Tukey boxplots (*B–F*, *H*, and *I*). $N = 12$ per treatment group. AU, arbitrary units; wk, weeks.

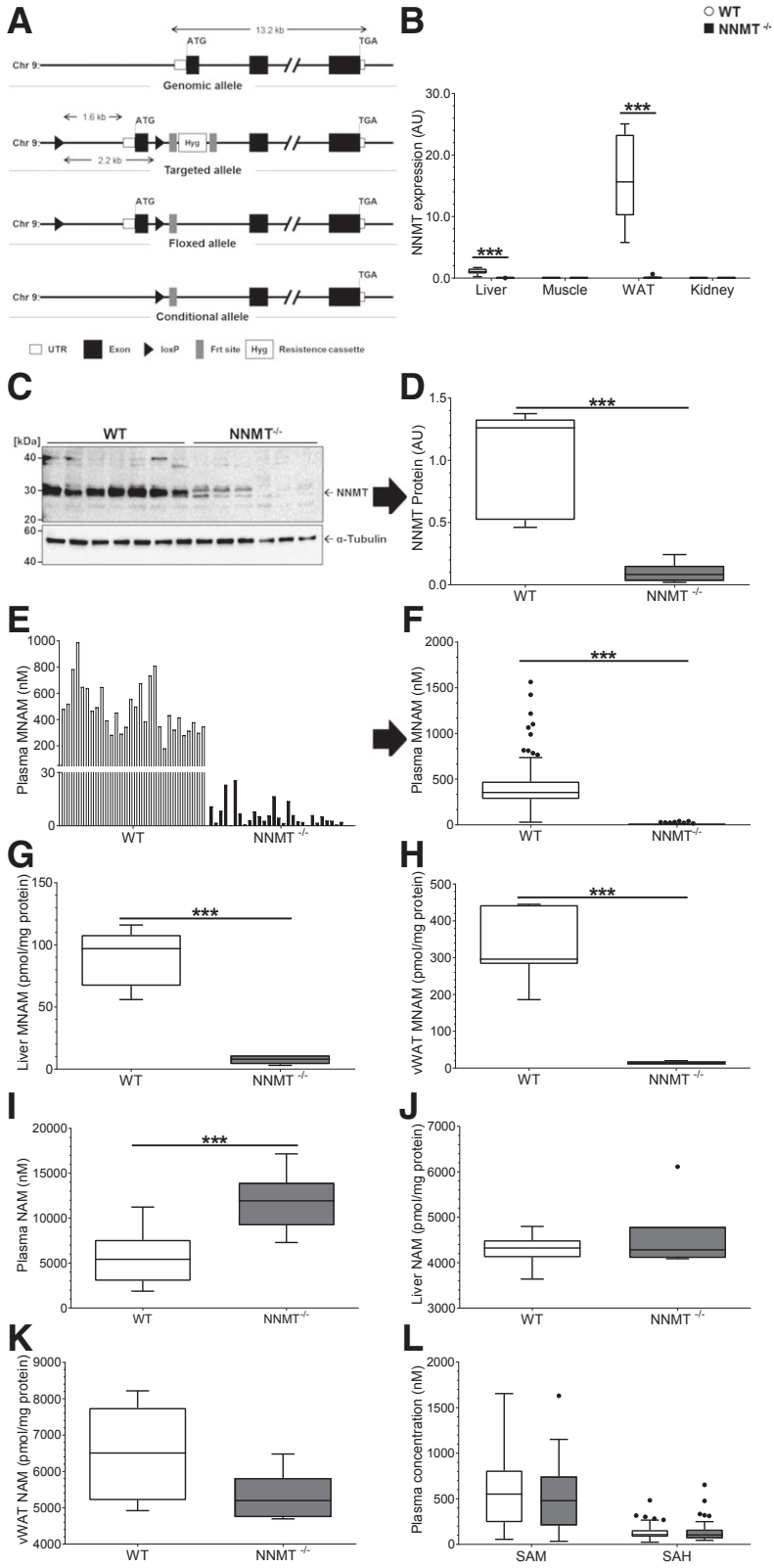

Figure 3—Generation and validation of an NNMT$^{-/-}$ mouse line. *A*: Strategy for *Nnmt* gene knockout with conditional potential. *B*: *Nnmt* expression in various tissues, all relative to WT liver, in NNMT$^{-/-}$ and WT male and female mice normalized to *β–actin* (liver), *Gapdh* (muscle), *Ppia* (WAT), and *Gapdh* (kidney). *N* = 14 (liver), *N* = 7 (muscle), *N* = 14 (WAT), *N* = 7 (kidney), each per genotype. *C*: Representative Western blot analysis of NNMT protein in vWAT of male mice. *D*: Relative quantification of NNMT protein normalized to α-tubulin. *N* = 6 per genotype. *E*: Concentration of MNAM in plasma of a representative sample of male and female WT and NNMT$^{-/-}$ mice; *N* = 30 per genotype. *F*: Plasma MNAM concentration: aggregate of male (*N* = 58/60) and female (*N* = 27/26) cohorts; *N* = 85/86 for WT/NNMT$^{-/-}$. MNAM concentration in liver tissue (*G*) and vWAT (*H*) of female mice; *N* = 7 per genotype. *I*: Level of plasma NAM of male (*N* = 35/37) and female (*N* = 20/19) mice;

Nnmt Deficiency in HFD-Fed Males Enhances IS but Not Glucose Tolerance

We next challenged NNMT$^{-/-}$ males that were fed an HFD, not a WD, for 10 weeks. No impact of *Nnmt* deletion on BW or composition was detected (Fig. 4*A*–*C*). Challenging the HFD-fed mice with glucose showed nearly identical glucose tolerance and similar insulin concentrations (Fig. 4*D* and *E*). In week 11, NNMT$^{-/-}$ mice were analyzed in metabolic cages. Both groups showed similar food and water intake (Fig. 4*F* and *G*). We did not reveal differences in O_2 consumption (data not shown), RER (Fig. 4*H*), or EE (Fig. 4*I*). Locomotor activity was low during the daytime and increased rapidly with the onset of nighttime, yet without significant differences (Fig. 4*J*).

Finally, we investigated the IS of HFD-fed mice by performing HE clamps. Conscious, restrained WT and NNMT$^{-/-}$ mice were clamped with similar mean steady-state plasma glucose concentrations (130 vs. 127 mg/dL) (Fig. 5*A*, top panel), whereas mean GIR was significantly elevated in NNMT$^{-/-}$ mice compared with WT mice (24 vs. 11 mg/kg/min), indicating improved IS in HFD-fed *Nnmt*-deficient mice (Fig. 5*A*, bottom panel). Plasma insulin level was comparable in either phase (Fig. 5*B*). Plasma NEFAs were similar in the basal phase, but insulin-mediated NEFA reduction was elevated in NNMT$^{-/-}$ mice (56%) compared with WT mice (33%) (Fig. 5*C*). Although basal EGP was similar (9 mg/kg/min), EGP under hyperinsulinemic conditions was almost completely suppressed in NNMT$^{-/-}$ mice, and WT mice showed only partial EGP reduction (23%) (Fig. 5*D*). Accordingly, R_d and glucose clearance were increased in NNMT$^{-/-}$ mice in the hyperinsulinemic phase, but not in the basal phase (Fig. 5*E* and *F*). Calculating the IS index (ISI) of the steady state, NNMT$^{-/-}$ mice showed a significant increase (0.28 mg/kg/min/[mU/L]) compared with WT (0.10 mg/kg/min/[mU/L], $P = 0.017$). The organ-specific glucose uptake (GU) in SKM and WAT revealed no significant difference; however, it did reveal a trend in SKM for NNMT$^{-/-}$ mice (Fig. 5*G*).

Despite similar body composition and glucose tolerance, HE clamp results strongly suggest substantially improved IS in HFD-fed NNMT$^{-/-}$ males with regard not only to insulin-stimulated GU but also to the inhibition of lipolysis and EGP.

Given reports that adipose SIRT1 (silent mating type information regulation 2 homolog 1) depletion may reduce IS (25–27), and that NNMT reduction may increase SIRT1 activity (12), we wondered whether increased SIRT1 may mediate the improved IS in NNMT$^{-/-}$ mice. However, adipose *Sirt1* expression, SIRT1 protein expression, and expression of target genes did not differ from those of controls (Fig. 5*H*–*J*). Hepatic SIRT1, *Sirt1*, and *G6pc* expression were not different from those of controls, whereas *Pck1* expression was increased in NNMT$^{-/-}$ mice (Fig. 5*H*–*J*). Analyzing representative respiratory chain complex genes/proteins as a proxy for cellular oxygen consumption in adipose tissue of NNMT$^{-/-}$ mice, we observed no significant differences (Fig. 5*K* and *L* and Supplementary Fig. 3).

Improved IS Cannot Be Explained by Regulation of Hepatic Gene Expression

To elucidate whether this enhanced IS is reflected in gene regulation, we performed RNA sequencing with liver samples of NNMT$^{-/-}$ and WT mice. However, between genotypes no obvious separation of both groups in the principal component analysis was observed, suggesting no fundamental regulatory difference (Supplementary Fig. 4). In detailed analysis, we found no highly differentially regulated genes aside from *Nnmt*, which was virtually absent in NNMT$^{-/-}$ (Supplementary Fig. 1*B*). All of the other 23 differentially expressed genes that exceeded cutoff were deemed unlikely to explain the observed HE clamp results (Supplementary Table 3).

Nnmt Deficiency in WD-Fed Females Improves BW and Composition but Not Glucose Tolerance

Finally, to corroborate our ASO-KD results, we analyzed NNMT$^{-/-}$ females during a 12-week WD, not an HFD, and observed decreased BW, with NNMT$^{-/-}$ mice finally weighing 6 g less than WT mice, whereas the initial BW and food intake did not differ (Fig. 6*A*–*C*). This was accounted for mainly by a difference in fat rather than lean mass (Fig. 6*D* and *E*). During a WD, fed glucose levels showed only a minor increase and remained comparable while insulin rose significantly less (37%) in NNMT$^{-/-}$ mice (Fig. 6*F*–*H*). However, *Nnmt* deletion did not reveal any benefit on glucose tolerance (Fig. 6*I*) and 15-min insulin measurement showed no significant difference investigated by oGTT (Fig. 6*J*). Likewise, other metabolic parameters such as NEFAs, triglycerides, cholesterol, HDL, and LDL analyzed in plasma did not differ between WD-fed WT and NNMT$^{-/-}$ females (data not shown). Fed with an HFD, female NNMT$^{-/-}$ mice did not show changes in BW and composition (data not shown).

NNMT and Its Metabolites in a Human WR Study

To explore the role of NNMT and its metabolites in humans and to check which findings from the mouse are transferrable, we analyzed data from a human WR study (23). Study participants were extensively characterized before (T-3) and after (T0) a 3-month WR intervention study. SKM and scWAT biopsy samples were taken and RNA sequenced (21,22).

$N = 55/56$ for WT/NNMT$^{-/-}$. NAM concentration in liver tissue (*J*) and vWAT (*K*) of female mice; $N = 7$ per genotype. *L*: Plasma concentration of SAM and SAH of male ($N = 35/37$) and female ($N = 20/19$) mice; $N = 55/56$ for WT/NNMT$^{-/-}$. White boxes/white bars depict WT mice; gray boxes/black bars depict NNMT$^{-/-}$ mice. $^{***}P \leq 0.001$. Statistical significance was calculated using two-tailed unpaired Student *t* test with Welch correction or Mann-Whitney test. Data represent Tukey boxplots (*B*, *D*, and *F*–*L*). AU, arbitrary units.

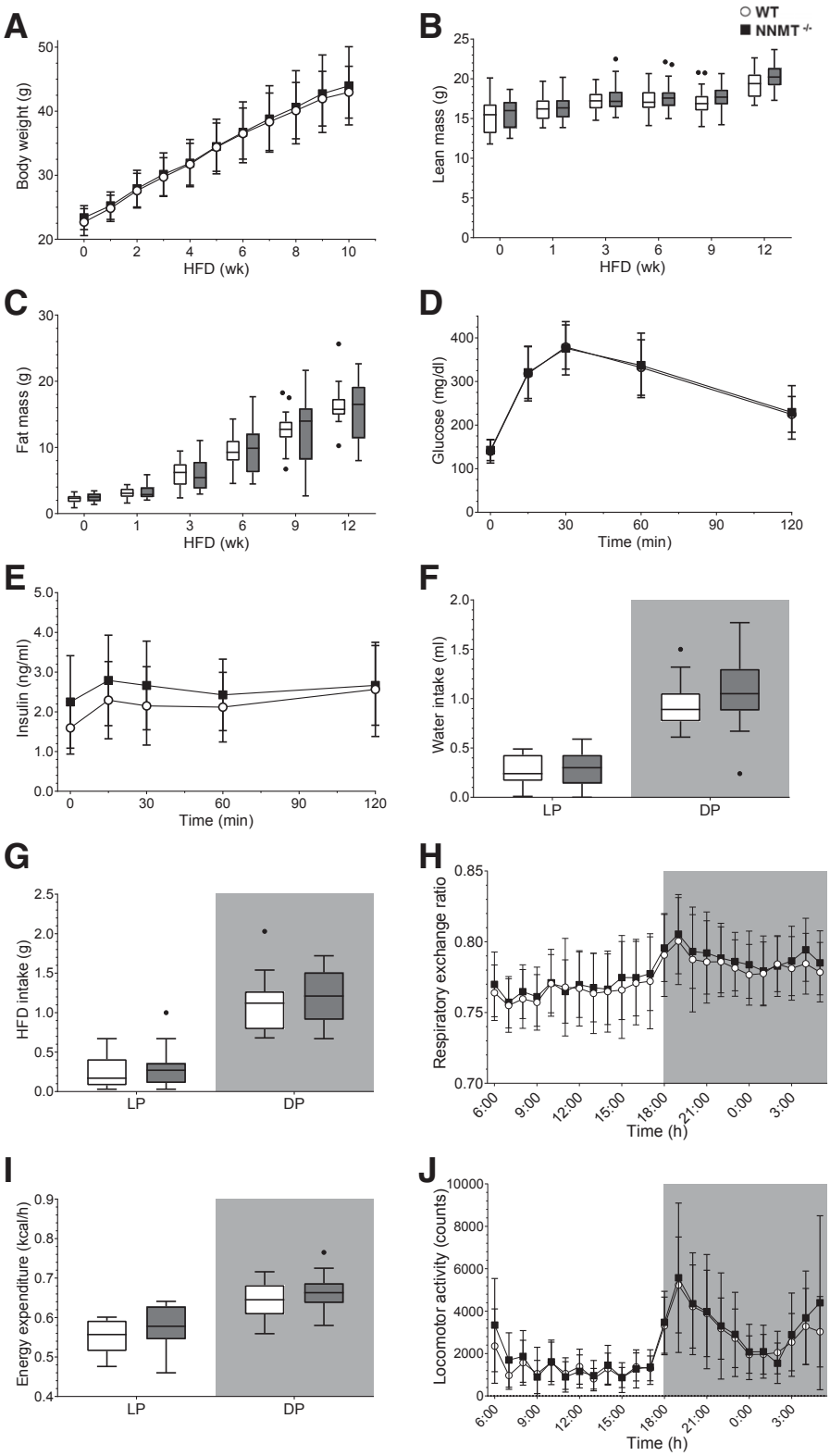

Figure 4—BW, body composition, parameters of glycemic control, and metabolic cage studies in male NNMT$^{-/-}$ and WT mice being fed an HFD. *A*: BW progression. *B*: Lean mass. *C*: Fat mass. *D*: Plasma glucose concentration during an ipGTT. *E*: Plasma insulin concentration during the ipGTT. *F*–*J*: Metabolic cage studies performed after 10 weeks of HFD. Water (*F*) and food (*G*) consumption during light (LP) and dark phase (DP). RER (*H*), EE in kilocalories per hour (*I*), and locomotor activity in counts (*J*). Gray background represents dark phase. White circles/white boxes depict WT mice; black squares/gray boxes depict NNMT$^{-/-}$ mice. Statistical significance was tested using two-way ANOVA with Bonferroni mct (*A*–*H* and *J*) and ANCOVAs with BW as a confounder (*I*). Data represent the mean ± SD (*A*, *D*, *E*, *H*, and *J*) or Tukey boxplots (*B*, *C*, *F*, *G*, and *I*). *N* = 32 (*A*–*C*), *N* = 20 (*D*–*J*). *N* values are stated per genotype. wk, weeks.

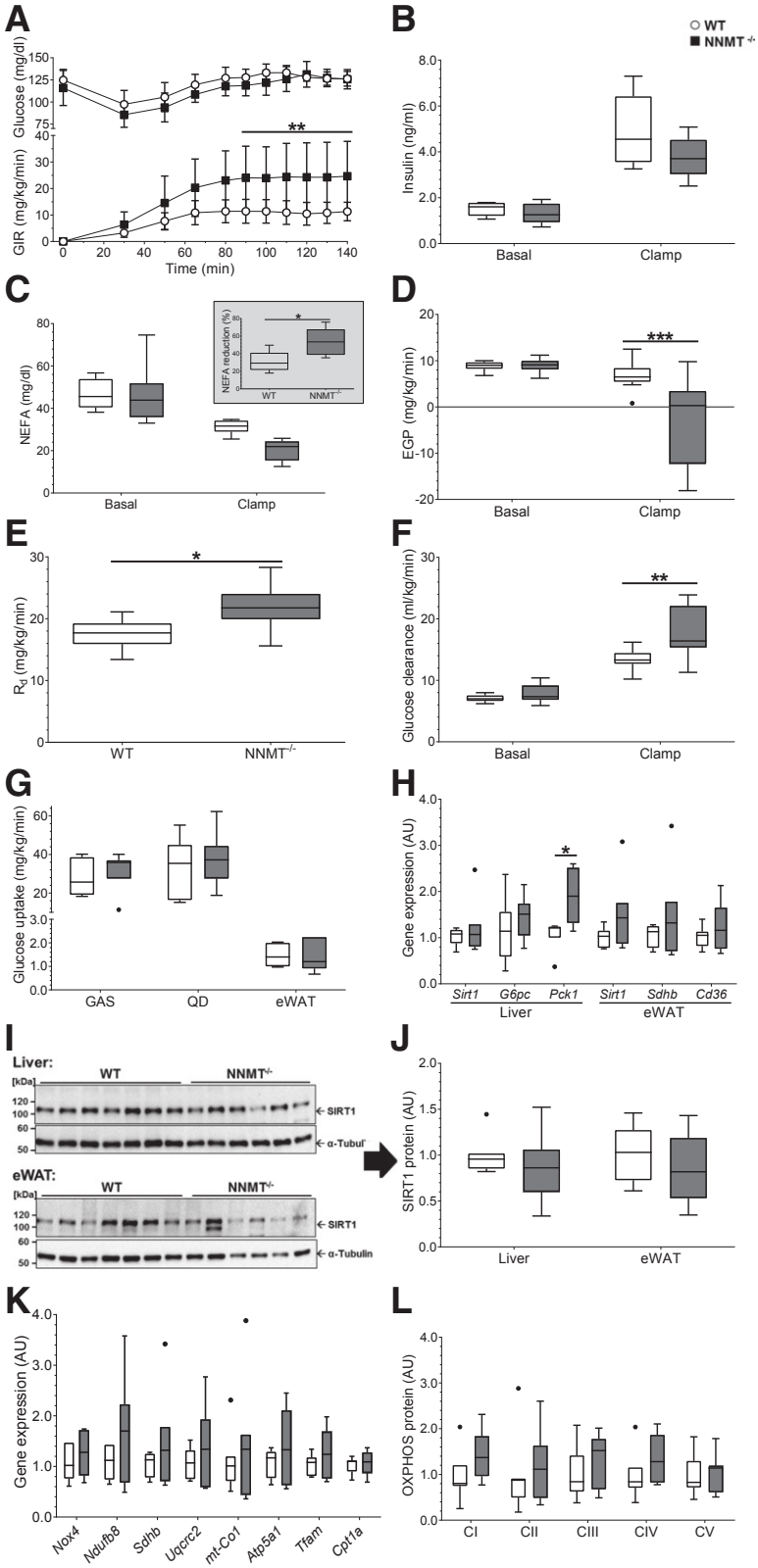

Figure 5—HE clamp analysis in conscious, restrained male NNMT$^{-/-}$ mice performed after 12 weeks of HFD. *A*: Plasma glucose concentration (top panel) and GIR (bottom panel) during HE clamp. *B*: Insulin concentration during basal and hyperinsulinemic steady-state (clamp) phase. *C*: Plasma concentrations of NEFAs in basal and clamp phase and their insulin-mediated reduction (in inset). *D*: EGP during basal and steady-state phase. *E*: R_d in steady-state phase. *F*: Glucose clearance during basal and clamp phase. *G*: Organ-specific GU in SKM (gastrocnemius [GAS] and quadriceps vastus lateralis [QD]) and eWAT. *H–L*: Gene and protein analysis of liver and eWAT from nonclamped NNMT$^{-/-}$ male mice fed an HFD for 12 weeks . *H*: Gene expression analysis of murine *Sirt1* (Sirtuin-1) and target genes such as hepatic *G6pc* (glucose-6-phosphatase catalytic-subunit) and *Pck1* (PEPCK 1) in liver and adipose *Sdhb* (succinate dehydrogenase complex

WR showed no differential regulation in SKM; however, the WR led to increased a*NNMT* (Fig. 7*A* and *B*), especially in 18- to 39- and 61- to 90-year-old subjects (Supplementary Fig. 5*A* and *B*). Before WR, a*NNMT* correlated negatively with IS, given by the ISI, or positively with HOMA-insulin resistance (IR), but these correlations disappeared after WR (Fig. 7*C* and *D*). Even after adjustment in a linear regression model with confounders (age, sex, BMI at T-3), the baseline correlation remained significant (ISI at T-3: $R = -0.299$, $P = 0.001$; HOMA-IR at T-3: $R = 0.324$, $P = 0.011$). No association between a*NNMT* and BMI, as a parameter for obesity, plasma NAM, or MNAM was present (Supplementary Fig. 5*C*–*E*). Both plasma NAM and MNAM were lower after WR (Fig. 7*E* and *F*). Neither NAM nor MNAM correlated with IS or BMI before WR. Surprisingly, despite the overall reduction, MNAM correlated positively with IS after WR (Fig. 7*G* and *H*), suggesting that those with the greatest reductions had lesser improvements in IS. In contrast, NAM correlated negatively with IS after WR (Supplementary Fig. 5*F* and *G*). A summary of findings from our WR study is found in Supplementary Table 4.

DISCUSSION

In female NNMT-ASO-KD mice fed a WD, we report reduced BW, fat, plasma glucose, and insulin and improved glucose tolerance. This is highly consistent with findings in male NNMT-ASO-KD mice reported by Kraus et al. (12). Building on this, we generated an *Nnmt*-deficient constitutive knockout mouse and demonstrated the deletion of *Nnmt* DNA, drastic reductions in RNA, and virtually no protein or MNAM; the faint protein band in vWAT may represent nonspecific antibody binding rather than residual amounts of NNMT protein. In WD-fed NNMT$^{-/-}$ females, we observed reduced BW, fat, and plasma insulin but no changes in glucose or glucose tolerance, whereas in HFD-fed NNMT$^{-/-}$ males we report increased IS under hyperinsulinemic conditions without changes in BW, fat, fasting glucose, fasting insulin, or glucose tolerance. This suggests a BW-independent modulation of IS in this group.

Our investigations add further evidence that a reduction of NNMT inhibits weight gain and protects against associated negative metabolic effects in models of diet-induced obesity. This may represent a viable pharmacological target for future treatment of such conditions (16,28,29). Consistent effects of NNMT-specific ASOs, small-molecule inhibition (12,16,28,29), and the genetic model described here provide strong evidence for the specificity of NNMT modulation.

An important, if somewhat surprising, finding is that complete genetic *Nnmt* deletion did not consistently meet all aspects of the obesity-resistant phenotype observed in NNMT-ASO-KD. NNMT$^{-/-}$ mice showed different responses depending on sex and detailed diet composition.

We confirmed that NNMT is the primary enzyme catalyzing the methylation of NAM and that this is not directly compensated by any other gene. It is, however, possible that epigenetic changes, mediated through altered metabolite concentrations during early development, are able to compensate for the NNMT loss on a system level and thus lead to metabolic normalization. In studies with ASOs or inhibitor, adult mice are used and, as such, this developmental window of opportunity may be missed (30). Alternatively, residual NNMT activity (10–40%) (12,16) may impede compensatory mechanisms that mediate adaptation to a null situation. Furthermore, it is possible that NNMT concentration within a certain range (in adipose or other tissues) is required to mediate the observed positive effects, whereas complete deletion negates these. Investigations of tissue-specific NNMT$^{-/-}$ mice could help to elucidate this and are currently underway.

An additional possibility is that some compensatory mechanisms are triggered upstream of the protein function (i.e., it may be the genetic mutation itself or the complete lack of transcript RNA rather than the loss of protein function that triggers these). In knockdown models, the DNA remains intact, and so such a compensatory mechanism would not be triggered (31). Similar discrepancies between ASO-KD and genetic knockout have previously been described (17,31–35).

We analyzed SIRT1 and several target genes in liver and eWAT of HFD-fed NNMT$^{-/-}$ males and compared the results with those previously published (9,12). We observed increased hepatic expression of *Pck1* in NNMT$^{-/-}$ mice, but no change in *Sirt1*, SIRT1 (protein), or *G6pc*,

iron sulfur subunit B) and *Cd36* (fatty acid translocase) in eWAT normalized to hepatic *Gapdh* and adipose *β-actin* as housekeeping genes. *I*: Western blot analysis of liver and eWAT for the detection of SIRT-1 and α-tubulin as a loading control. *J*: Densitometric quantification of *I*. *K*: Gene expression analysis of murine mitochondrial respiratory chain complexes in adipose tissue (eWAT); for complex I *Nox4* (NADPH oxidase 4) and *Ndufb8* (NADH:ubiquinone oxidoreductase subunit B8), for complex II *Sdhb*, for complex III *Uqcrc2* (ubiquinol-cytochrome C reductase core protein 2), for complex IV *mt-Co1* (mitochondrially encoded cytochrome C oxidase I), as well as for complex V *Atp5a1* (ATP synthase, H^+ transporting, mitochondrial F1 complex, α subunit 1) and further *Tfam* (mitochondrial transcription factor 1) and *Cpt1a* (mitochondrial carnitine palmitoyltransferase 1a) were measured and normalized to adipose *β-Actin* as a housekeeping gene. *L*: Quantification of Western blot analysis of the respiratory chain complexes in eWAT. Protein concentrations of complex I (CI: NDUFB8), complex II (CII: SDHB), complex III (CIII: MTCO1), complex IV (CIV: UQCRC2), and complex V (CV: ATP5A) were quantified and standardized to GAPDH as a loading control. Original Western blot analysis is depicted in Supplementary Fig. 3. White circles/white boxes depict WT mice; black squares/gray boxes depict NNMT$^{-/-}$ mice. $^*P \leq 0.05$, $^{**}P \leq 0.01$, $^{***}P \leq 0.001$. Statistical significance was calculated using two-way ANOVA with Bonferroni mct (*A*, *B*, *D*, *F*, *H*, *K*, and *L*) or two-tailed unpaired Student *t* test with Welch correction or Mann-Whitney test (*C*, *E*, *G*, and *J*). Data represent the mean ± SD (*A*) or Tukey boxplots (*B–H* and *J–L*). $N = 9/8$ (*A–G*). $N = 7/6$ (*H–L*). *N* values are stated per genotype, with WT shown first. AU, arbitrary units.

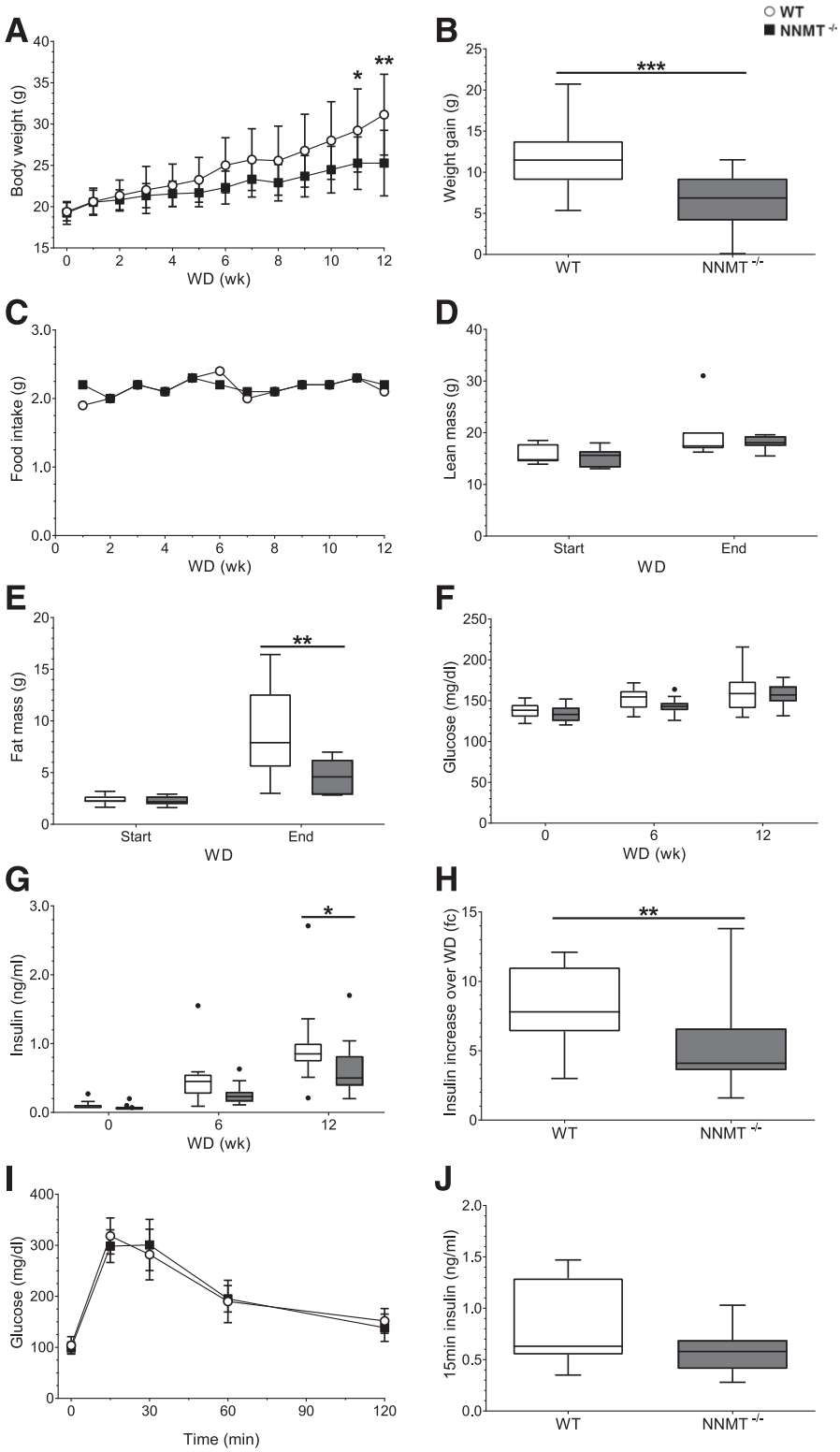

Figure 6— BW, body composition, and parameters of glycemic control in female NNMT$^{-/-}$ and WT mice during a 12-week WD. *A*: BW progression. *B*: Total BW gain after a 12-week WD. *C*: Food intake was measured weekly for each cage and was calculated per mouse. *D*: Lean mass. *E*: Fat mass. Plasma glucose (*F*) and insulin (*G*) concentration in ad libitum–fed mice. *H*: Increase of insulin in ad libitum–fed state over a 12-week WD (fold-change [fc] compared with week 0). *I*: Plasma glucose concentration during an oGTT. *J*: Measurement of plasma insulin at 15 min within the oGTT. White circles/white boxes depict WT; black squares/gray boxes depict NNMT$^{-/-}$ mice. *$P \leq 0.05$, **$P \leq 0.01$, ***$P \leq 0.001$. Statistical significance was calculated using a two-tailed unpaired Student *t* test with Welch correction (*B*), Mann-Whitney test (*H* and *J*), or two-way ANOVA with Bonferroni mct (*A*, *D*–*G*, and *I*). Data represent the mean (*C*) ± SD (*A* and *I*) or Tukey boxplots (*B* and *D*–*J*). *N* = 15 (*A*–*C* and *F*–*H*), *N* = 7 (*D*, *E*, *I*, and *J*). *N* values are stated per genotype. wk, weeks.

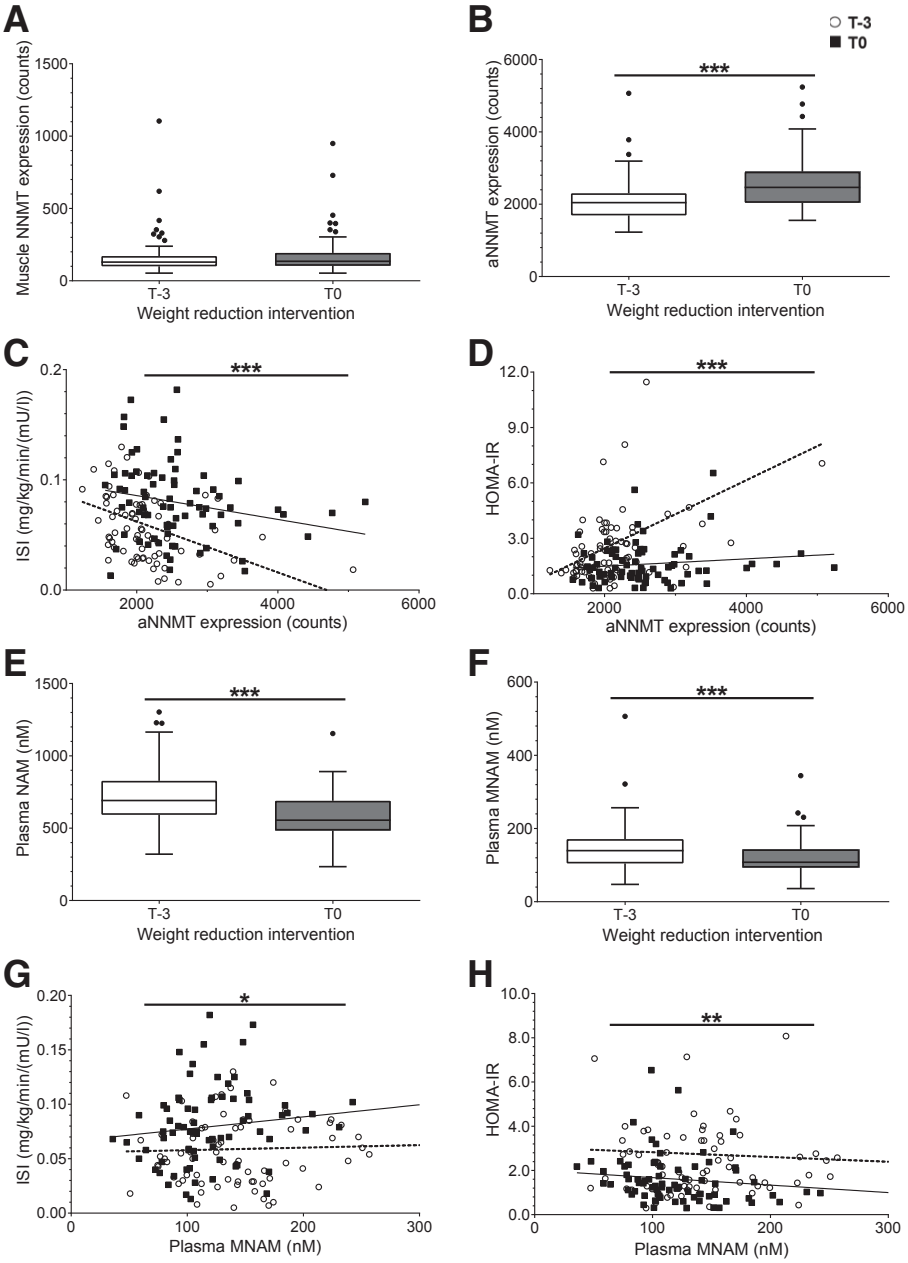

Figure 7—*NNMT* expression, its substrate NAM, and its product MNAM and their correlations with metabolic parameters before (T-3) and after (T0) a human WR intervention study. *A*: Human *NNMT* RNA expression from SKM (gastrocnemius) biopsy samples assessed via next-generation sequencing. $N = 87$ for muscle biopsy samples. *B*: Human *NNMT* RNA expression in scWAT biopsy samples. *C*: Spearman correlation of a*NNMT* expression with ISI. A correlation was observed before WR ($R = -0.439$, $P = 0.001$) but not after WR ($R = -0.233$, $P = 0.312$). *D*: Spearman correlation of a*NNMT* expression with HOMA-IR. A correlation was observed before WR ($R = 0.385$, $P = 0.005$) but not after WR ($R = -0.086$, $P = 1.0$). *E*: NAM concentrations in human plasma samples. *F*: Human plasma MNAM levels before and after WR. *G*: Spearman correlation of plasma MNAM with ISI. A correlation was not observed before WR ($R = -0.047$, $P = 0.687$) but was observed after WR ($R = 0.250$, $P = 0.031$). *H*: Spearman correlation of plasma MNAM with HOMA-IR. A correlation was not observed before WR ($R = 0.024$, $P = 0.837$) but was observed after WR ($R = -0.305$, $P = 0.008$). White circles/white boxes depict 3 months before (T-3) WR; black squares/gray boxes depict after (T0) WR. $^{*}P \leq 0.05$, $^{**}P \leq 0.01$, $^{***}P \leq 0.001$. Statistical significance was calculated using a two-tailed Wilcoxon matched-pairs signed rank test (*B*, *E*, and *F*) and Spearman correlation with Bonferroni adjustment for multiple testing (*C*, *D*, *G*, and *H*). Data represent Tukey boxplots (*A*, *B*, *E*, and *F*) or Spearman correlation (*C*, *D*, *G*, and *H*). $N = 75$ for adipose tissue biopsies (*B*–*H*).

whereas Hong et al. (9) reported reduced SIRT1 and *G6pc* in NNMT-KD mice but unchanged *Sirt1* and *Pck1*, and Kraus et al. (12) reported reduced *Sirt1* but unchanged *Pck1* and *G6pc*. In WAT, Kraus et al. (12) reported increased expression of SIRT1 target genes *Cd36*, *Cat*, and *Sdhb*. We also measured these along with *Sirt1* and SIRT1 but did not reveal any differences between $NNMT^{-/-}$ and WT mice. Our data, therefore, do not directly support the hypothesis that NNMT, through its product MNAM, increases the stability of SIRT1 protein as in the study

by Hong et al. (9). The discrepancies among these three works highlight the need for further investigations.

Compared with the study by Kraus et al. (12), we additionally included a vehicle-control to control-ASO and NNMT-ASO and found an effect of control-ASO compared with vehicle (Fig. 1). This could indicate a general (energy-consuming) RNA interference effect responding to the exogenous scrambled siRNA, but not to vehicle-only (36–39), alongside the NNMT metabolic effects that are missed without vehicle.

Sex and age differences in DNA methylation starting at 4 weeks and a gradual establishment of sex-dependent hypomethylation were reported for the l*Nnmt* gene among others (40). This may also occur in other tissues and could explain the sex differences in response to diet and also differences between ASO-KD and knockout mice. l*Nnmt* expression showed sex differences in mice with an altered methylation pattern in which l*Nnmt* levels were lower in males (40). Because NNMT is also involved in histone methylation via SAM (30) and histone methylation can also be sex specific, the deletion of *Nnmt* could also lead to sex differences in the methylation pattern and, therefore, produce different responses between $NNMT^{-/-}$ males and females per se, and in particular in response to different diets. Beyond that, a limitation of our investigation is the use of different diets for males and females. Male mice were fed an HFD, whereas females were fed a WD, resulting in more calories originating from carbohydrates (Supplementary Tables 6 and 7). Simply, this could underlie the differences observed between sexes (41). Further research on $NNMT^{-/-}$ mice is warranted to fully elucidate whether sex and/or the dietary nutrient content underlie the observed differences.

Despite unchanged glucose tolerance, we observed markedly improved IS in male $NNMT^{-/-}$ mice being fed an HFD investigated in an HE clamp. Both increased R_d and sustained insulin-mediated suppression of EGP contributed to the higher GIR in $NNMT^{-/-}$ mice. Additionally, in the distinct SKM and adipose tissues tested, a trend for but no significant difference in GU was observed. It is likely that a summation effect and possibly increased hepatic GU may be responsible for the significantly elevated R_d (Fig. 5). Because improved IS could not be explained by differences in hepatic gene regulation (Supplementary Table 7), extrahepatic processes or post-translational and/or flux regulation mediated by MNAM may contribute to the improved IS without affecting steady-state gene expression.

Several plausible mechanisms have been proposed through which increased NNMT activity could mediate either the development of, or protection against, obesity and loss of IS. For instance, increased plasma MNAM may induce inflammation and insulin resistance (2,8). Otherwise, studies have shown MNAM to have antithrombotic and anti-inflammatory effects, to lower plasma triglycerides, and to protect against endothelial dysfunction (42), and it is implicated in mediating extended life span in *Caenorhabditis elegans* (43). Other mechanisms through which NNMT activity might regulate energy metabolism are the modulation of NAD^+ synthesis affecting $NAD(P)^+$ concentration and $NAD(P)^+$/NAD(P)H ratio, changes in cellular methylation potential (SAM/SAH ratio), or reduction in polyamine flux.

A distinct β-cell phenotype of $NNMT^{-/-}$ mice could explain the discrepancy of improved IS without enhanced glucose tolerance due to an altered modulation of insulin secretion. An important difference of the whole-body *Nnmt* deletion is that it also affects pancreatic islets, whereas the NNMT-ASO-KD does not. However, this was not observed during the glucose challenge of $NNMT^{-/-}$ mice, and merely an impaired insulin secretion could be causative (Fig. 6*G* and *H*). Additionally, in PANC-1 cells, a pancreatic cancer cell line, NNMT-ASO-KD reduced cell proliferation and survival under metabolic stress (44).

Consistent with a study involving obese adults (2), we observed no correlations between BW/fat and MNAM in our human study. Our negative correlation between a*NNMT* and IS is in agreement with the study by Kannt et al. (2) and the idea that increased a*NNMT* expression/activity is associated with insulin resistance. The increased a*NNMT* as a result of WR is somewhat surprising but is not in direct contradiction with previously published data, which showed a decrease only in subjects with T2D or impaired glucose tolerance after a 12-week exercise program (2). Another study (45) found increased *NNMT* in SKM and elevated plasma MNAM after a short and intense WR intervention study. Indeed, after WR and contrary to expectations (2,46), MNAM correlated positively with ISI. The fact that a correlation between *NNMT* and IS disappeared after WR and that correlations between the metabolites NAM, MNAM, and IS appeared only after WR is surprising and points to a complex regulation of these metabolites. This remains to be elucidated.

Acknowledgments. The authors thank Diana Woellner (Charité–Universitätsmedizin Berlin, Berlin, Germany, and DZHK [German Centre for Cardiovascular Research], partner site Berlin) and Marie-Christin Gaerz (Charité–Universitätsmedizin Berlin) for assistance in (mouse) experiments; Nadine Huckauf (Charité–Universitätsmedizin Berlin) and Candy Kalischke (Charité–Universitätsmedizin Berlin) for assistance with biochemical experiments and quantitative PCR; and Hui Tang (Charité–Universitätsmedizin Berlin) for assistance during HE clamps. The authors also thank Beate Greiner (Sanofi Research and Development, Frankfurt am Main, Germany) for large-scale synthesis of the ASOs; Mostafa Kabiri (Sanofi Research and Development) for help with design, generation, and breeding of the conditional $NNMT^{-/-}$ mouse strain; Gitte Hansen (Gubra ApS, Hørsholm, Denmark) for conducting the ASO study; and Claire Kammermeier (Sanofi Research and Development), Martin Stephan (Sanofi Research and Development), Pierre Wenski (Sanofi Research and Development), Jörn Wandschneider (Sanofi Research and Development), Uwe Butty (Sanofi Research and Development), Mandy Grohmann (Sanofi Research and Development), and Kerstin Lentz (Sanofi Research and Development) for technical assistance. The Genotype-Tissue Expression (GTEx) Project was supported by the Common Fund of the Office of the Director of the National Institutes of Health and by the National Cancer Institute; National Human Genome Research Institute; National Heart, Lung, and Blood Institute; National Institute on Drug Abuse; National Institute of Mental Health; and National Institute

of Neurological Disorders and Stroke. The expression data for human *NNMT* described in the Introduction were obtained from the GTEx Portal on 15 January 2018.

Funding. This work was supported by a joint laboratory between Charité and Sanofi, Deutsches Zentrum für Herz-Kreislauf-Forschung (DZHK/BMBF), the ICEMED Consortium, and the Berlin Institute of Health.

Duality of Interest. S.B., K.M., and J.S. received research support in relation to the joint laboratory between Charité–Universitätsmedizin Berlin and Sanofi. M.B. is an employee of Treamid Therapeutics GmbH. K.J.-H., R.E., A.P., F.B., D.M., and A.K. are employees of Sanofi. No other potential conflicts of interest relevant to this article were reported.

Author Contributions. S.B. designed the studies; performed experiments; contributed to discussion of the results; supervised the project; and wrote, critically reviewed, and edited the manuscript. J.P. performed experiements; contributed to discussion of the results; and wrote, critically reviewed, and edited the manuscript. M.B. performed experiments, analyzed the clinical study data, contributed to discussion of the results, and critically reviewed the manuscript. K.J.-H. designed and synthetized the ASOs. R.E., A.P., and F.B. performed experiments. D.M. analyzed mouse next-generation sequencing data. K.M. performed experiments, assessed and analyzed the clinical study data, contributed to discussion of the results, and critically reviewed the manuscript. J.S. designed the studies, supervised the project, assessed the clinical study, contributed to discussion of the results, and critically reviewed and edited the manuscript. A.K. designed the studies, supervised the project, performed experiments, contributed to discussion of the results, and critically reviewed and edited the manuscript. S.B. is the guarantor of this work and, as such, had full access to all the data in the study and takes responsibility for the integrity of the data and the accuracy of the data analysis.

Prior Presentation. Parts of this study were presented in abstract form at the 78th Scientific Sessions of the American Diabetes Association, Orlando, FL, 22–26 June 2018.

References

1. Bromberg A, Levine J, Belmaker R, Agam G. Hyperhomocysteinemia does not affect global DNA methylation and nicotinamide N-methyltransferase expression in mice. J Psychopharmacol 2011;25:976–981
2. Kannt A, Pfenninger A, Teichert L, et al. Association of nicotinamide-N-methyltransferase mRNA expression in human adipose tissue and the plasma concentration of its product, 1-methylnicotinamide, with insulin resistance. Diabetologia 2015;58:799–808
3. GTEx Consortium. The genotype-tissue expression (GTEx) project. Nat Genet 2013;45:580–585
4. Riederer M, Erwa W, Zimmermann R, Frank S, Zechner R. Adipose tissue as a source of nicotinamide N-methyltransferase and homocysteine. Atherosclerosis 2009;204:412–417
5. Ulanovskaya OA, Zuhl AM, Cravatt BF. NNMT promotes epigenetic remodeling in cancer by creating a metabolic methylation sink. Nat Chem Biol 2013;9:300–306
6. Alston TA, Abeles RH. Substrate specificity of nicotinamide methyltransferase isolated from porcine liver. Arch Biochem Biophys 1988;260:601–608
7. Aksoy S, Szumlanski CL, Weinshilboum RM. Human liver nicotinamide N-methyltransferase. cDNA cloning, expression, and biochemical characterization. J Biol Chem 1994;269:14835–14840
8. Zhou SS, Li D, Sun WP, et al. Nicotinamide overload may play a role in the development of type 2 diabetes. World J Gastroenterol 2009;15:5674–5684
9. Hong S, Moreno-Navarrete JM, Wei X, et al. Nicotinamide N-methyltransferase regulates hepatic nutrient metabolism through Sirt1 protein stabilization. Nat Med 2015;21:887–894
10. Salek RM, Maguire ML, Bentley E, et al. A metabolomic comparison of urinary changes in type 2 diabetes in mouse, rat, and human. Physiol Genomics 2007;29:99–108
11. Teperino R, Schoonjans K, Auwerx J. Histone methyl transferases and demethylases; can they link metabolism and transcription? Cell Metab 2010;12:321–327
12. Kraus D, Yang Q, Kong D, et al. Nicotinamide N-methyltransferase knockdown protects against diet-induced obesity. Nature 2014;508:258–262
13. Drew JE, Farquharson AJ, Horgan GW, Williams LM. Tissue-specific regulation of sirtuin and nicotinamide adenine dinucleotide biosynthetic pathways identified in C57Bl/6 mice in response to high-fat feeding. J Nutr Biochem 2016;37:20–29
14. Lee YH, Nair S, Rousseau E, et al. Microarray profiling of isolated abdominal subcutaneous adipocytes from obese vs non-obese Pima Indians: increased expression of inflammation-related genes. Diabetologia 2005;48:1776–1783
15. Valenzuela DM, Murphy AJ, Frendewey D, et al. High-throughput engineering of the mouse genome coupled with high-resolution expression analysis. Nat Biotechnol 2003;21:652–659
16. Kannt A, Rajagopal S, Kadnur SV, et al. A small molecule inhibitor of nicotinamide N-methyltransferase for the treatment of metabolic disorders. Sci Rep 2018;8:3660
17. Brachs S, Winkel AF, Tang H, et al. Inhibition of citrate cotransporter Slc13a5/mINDY by RNAi improves hepatic insulin sensitivity and prevents diet-induced non-alcoholic fatty liver disease in mice. Mol Metab 2016;5:1072–1082
18. Brachs S, Lang C, Buslei R, et al. Monoclonal antibodies to discriminate the EF hand containing calcium binding adaptor proteins EFhd1 and EFhd2. Monoclon Antib Immunodiagn Immunother 2013;32:237–245
19. Morowski M, Brachs S, Mielenz D, Nieswandt B, Dütting S. The adaptor protein Swiprosin-1/EFhd2 is dispensable for platelet function in mice. PLoS One 2014;9:e107139
20. Schneider CA, Rasband WS, Eliceiri KW. NIH Image to ImageJ: 25 years of image analysis. Nat Methods 2012;9:671–675
21. Brachs M, Wiegand S, Leupelt V, et al. ANP system activity predicts variability of fat mass reduction and insulin sensitivity during weight loss. Metabolism 2016;65:935–943
22. Mai K, Brachs M, Leupelt V, et al. Effects of a combined dietary, exercise and behavioral intervention and sympathetic system on body weight maintenance after intended weight loss: results of a randomized controlled trial. Metabolism 2018;83:60–67
23. Mai K, Li L, Wiegand S, et al. An integrated understanding of the molecular mechanisms how adipose tissue metabolism affects long-term body weight maintenance. Diabetes 2019;68:57–65
24. R Core Team. *The R Project for Statistical Computing. Version. 3.1.1*, Vienna, Austria, R Foundation for Statistical Computing, 2014
25. Yoshizaki T, Milne JC, Imamura T, et al. SIRT1 exerts anti-inflammatory effects and improves insulin sensitivity in adipocytes. Mol Cell Biol 2009;29:1363–1374
26. Chalkiadaki A, Guarente L. High-fat diet triggers inflammation-induced cleavage of SIRT1 in adipose tissue to promote metabolic dysfunction. Cell Metab 2012;16:180–188
27. Cao Y, Jiang X, Ma H, Wang Y, Xue P, Liu Y. SIRT1 and insulin resistance. J Diabetes Complications 2016;30:178–183
28. Ruf S, Hallur MS, Anchan NK, et al. Novel nicotinamide analog as inhibitor of nicotinamide N-methyltransferase. Bioorg Med Chem Lett 2018;28:922–925
29. Neelakantan H, Vance V, Wetzel MD, et al. Selective and membrane-permeable small molecule inhibitors of nicotinamide N-methyltransferase reverse high fat diet-induced obesity in mice. Biochem Pharmacol 2018;147:141–152
30. Sperber H, Mathieu J, Wang Y, et al. The metabolome regulates the epigenetic landscape during naive-to-primed human embryonic stem cell transition. Nat Cell Biol 2015;17:1523–1535
31. Rossi A, Kontarakis Z, Gerri C, et al. Genetic compensation induced by deleterious mutations but not gene knockdowns. Nature 2015;524:230–233
32. Brachs S, Winkel AF, Polack J, et al. Chronic activation of hepatic Nrf2 has no major effect on fatty acid and glucose metabolism in adult mice. PLoS One 2016;11:e0166110

33. Kok FO, Shin M, Ni CW, et al. Reverse genetic screening reveals poor correlation between morpholino-induced and mutant phenotypes in zebrafish. Dev Cell 2015;32:97–108
34. Karakas B, Weeraratna AT, Abukhdeir AM, et al. P21 gene knock down does not identify genetic effectors seen with gene knock out. Cancer Biol Ther 2007;6:1025–1030
35. De Souza AT, Dai X, Spencer AG, et al. Transcriptional and phenotypic comparisons of Ppara knockout and siRNA knockdown mice. Nucleic Acids Res 2006;34:4486–4494
36. Nykänen A, Haley B, Zamore PD. ATP requirements and small interfering RNA structure in the RNA interference pathway. Cell 2001;107:309–321
37. Scacheri PC, Rozenblatt-Rosen O, Caplen NJ, et al. Short interfering RNAs can induce unexpected and divergent changes in the levels of untargeted proteins in mammalian cells. Proc Natl Acad Sci U S A 2004;101:1892–1897
38. Sledz CA, Holko M, de Veer MJ, Silverman RH, Williams BR. Activation of the interferon system by short-interfering RNAs. Nat Cell Biol 2003;5:834–839
39. Raof NA, Rajamani D, Chu HC, et al. The effects of transfection reagent polyethyleneimine (PEI) and non-targeting control siRNAs on global gene expression in human aortic smooth muscle cells. BMC Genomics 2016;17:20
40. Takasugi M, Hayakawa K, Arai D, Shiota K. Age- and sex-dependent DNA hypomethylation controlled by growth hormone in mouse liver. Mech Ageing Dev 2013;134:331–337
41. Dobner J, Ress C, Rufinatscha K, et al. Fat-enriched rather than high-fructose diets promote whitening of adipose tissue in a sex-dependent manner. J Nutr Biochem 2017;49:22–29
42. Houtkooper RH, Cantó C, Wanders RJ, Auwerx J. The secret life of NAD+: an old metabolite controlling new metabolic signaling pathways. Endocr Rev 2010;31:194–223
43. Schmeisser K, Mansfeld J, Kuhlow D, et al. Role of sirtuins in lifespan regulation is linked to methylation of nicotinamide. Nat Chem Biol 2013;9:693–700
44. Yu T, Wang YT, Chen P, et al. Effects of nicotinamide N-methyltransferase on PANC-1 cells proliferation, metastatic potential and survival under metabolic stress. Cell Physiol Biochem 2015;35:710–721
45. Ström K, Morales-Alamo D, Ottosson F, et al. N^1-methylnicotinamide is a signalling molecule produced in skeletal muscle coordinating energy metabolism. Sci Rep 2018;8:3016
46. Liu M, Li L, Chu J, et al. Serum N(1)-methylnicotinamide is associated with obesity and diabetes in Chinese. J Clin Endocrinol Metab 2015;100:3112–3117